Author Manuscript

Author Manuscript

Author Manuscript

Author Manuscript

HHS Public Access

Author manuscript

Mol Imaging Biol. Author manuscript; available in PMC 2016 October 01.

Published in final edited form as:

Mol Imaging Biol. 2015 October ; 17(5): 671–679. doi:10.1007/s11307-015-0842-8.

Utilizing the Multiradionuclide Resolving Power of SPECT and Dual Radiolabeled Single Molecules to Assess Treatment Response of Tumors

Baogang Xu, **Monica Shokeen**, **Gail P. Sudlow**, **Scott E. Harpstrite**, **Kexian Liang**, **Philip P. Cheney**, **W. Barry Edwards**, **Vijay Sharma**, **Richard Laforest**, **Walter J. Akers**, and **Samuel Achilefu**

Mallinckrodt Institute of Radiology, Washington University School of Medicine, 4525 Scott Avenue, St. Louis, MO, 63110, USA

Abstract

Purpose—Single photon emission computed tomography (SPECT) radionuclide pairs having distinct decay rates and different energy maxima enable simultaneous detection of dual gamma signals and real-time assessment of dynamic functional and molecular processes *in vivo*. Here, we report image acquisition and quantification protocols for a single molecule labeled with two different radionuclides for functional SPECT imaging.

Procedures—LS370 and LS734 were prepared using modular solid phase peptide synthesis. Each agent has a caspase-3 cleavable reporting motif, flanked by a tyrosine residue and a chelator at the opposite end of molecule. Cell uptake and efflux were assessed in human MDA-MB-231 breast cancer cells. Biodistribution studies were conducted in tumor naive and orthotopic 4T1 metastatic breast cancer tumor mice. NanoSPECT dual-imaging validation and attenuation correction parameters were developed using phantom vials containing varying radionuclide concentrations. Proof-of-principle SPECT imaging was performed in MMTV-PyMT transgenic mice.

Results—LS370 and LS734 were singly or dually radiolabeled with ^{125}I and ^{111}In or ^{99m}Tc. Cell assays demonstrated 11-fold higher percent uptake (P<0.001) of [^{125}I]LS734 (3.6±0.5) compared to [^{125}I]LS370 (0.3±0.3) at 2 h. Following chemotherapy, cellular retention of [^{125}I]LS734 was 3-fold higher (P<0.05) than untreated cells. Pharmacokinetics at 1 h postinjection demonstrated longer blood retention (%ID/g) for [^{125}I]LS734 (3.2±0.9) compared to [^{125}I]LS370 (1.6±0.1). In mice bearing bilateral orthotopic 4T1 tumors, the uptake (%ID/g) was 2.4±0.3 for [^{125}I]LS734 and 1.2±0.03 for [^{125}I]LS370. The iodinated tyrosine peptide residue label was stable under *in vitro* conditions for up to 24 h; rapid systemic deiodination (high thyroid uptake) was observed *in vivo*. Phantom studies using standards demonstrated deconvolution of radionuclide signals based on

Correspondence to: Samuel Achilefu; achilefus@mir.wustl.edu.

Electronic supplementary material The online version of this article (doi:10.1007/s11307-015-0842-8) contains supplementary material, which is available to authorized users.

Ethical Approval. All procedures performed in studies involving human participants were in accordance with the ethical standards of the institutional and/or national research committee and with the 1964 Helsinki declaration and its later amendments or comparable ethical standards.

Conflict of Interest. The authors declare that they have no conflict of interest.

Author Manuscript Author Manuscript Author Manuscript Author Manuscript

different gamma ray energies. In MMTV-PyMT mice imaged with dual-labeled [^{111}In]–[^{125}I]LS734, the gamma signals were separable and quantifiable.

Conclusions—Image processing protocols were developed for quantitative signal separation resulting from a caspase-3 responsive dual-radiolabeled SPECT probe. Crosstalk unmixing was obtained for multiradionuclide NanoSPECT imaging. *In vitro* and in vivo data demonstrated structure–activity relationships for developing functional agents for ratiometric SPECT imaging.

Keywords

Cancer; Apoptosis; Caspase; Programmed cell death; Radionuclide; SPECT; Cleavable peptide

Introduction

There are many molecular processes involved in cancer progression. The development of molecular therapies and imaging agents targeted to distinct pathological pathways has raised hope for early cancer detection and individualized therapy. An important biomarker of cancer is the diagnostic and prognostic family of proteases [1]. Although they play key roles in normal human physiology, their aberrant expression in cancer results in many undesirable effects such as an increase in tumor proliferation, metastasis, and resistance to therapy. As a result, new targeted therapies have been developed for specifically inhibiting these enzymes in cancer patients. A particularly interesting biochemical event is the migration of some proteases to unusual extracellular or intracellular spaces under pathological conditions, where they exert their cancer-supporting roles [2, 3]. In this regard, a combination of quantitative detection of protein expression, localization, and functional status is required for accurate cancer diagnosis and assessment of response to therapy.

Clinically, positron emission tomography (PET) and single photon emission tomography (SPECT) are the molecular imaging techniques of choice because of their high sensitivity and whole-body quantitative imaging capabilities [4]. Elegant methods have been developed to improve *in vivo* detection sensitivity of predictive enzymes by PET, including the use of [^{18}F]fluorothymidine to report cell proliferation *via* the activity of thymidine kinase-1 [5]. Despite the unique advantages of these nuclear imaging methods, their applications in molecular imaging have been confined to receptor-targeted imaging of cancer [4] or indirect reporting of the functional status of proteases *in vivo* by use of radiolabeled inhibitors [6]. Currently, there are no nuclear imaging agents for assessing the functional status of intracellular proteases *in vivo*.

Unlike PET, where all annihilation photons detected have the same energy (511 keV), which precludes simultaneous discrimination of multiple PET radionuclides from the same tracer, SPECT has multiradionuclide-resolving power. This is because the gamma cameras used in SPECT can acquire projection data simultaneously from two or more radionuclides in separate energy windows with resolution exceeding that of micro-PET [7]. In addition to differences ^{in} the emission energies, radionuclides amenable for SPECT imaging have sufficiently long half-lives for timely transportation, and can be produced on site *via* generators. The long half-lives of commonly used SPECT radionuclides, such as ^{99m}Tc ($t_{1/2}$, 6.02 h), ^{123}I ($t_{1/2}$, 13.2 h), ^{125}I ($t_{1/2}$, 59.4 days), and ^{111}In ($t_{1/2}$, 2.8 days), make them

Author Manuscript Author Manuscript Author Manuscript Author Manuscript

suitable for incorporation into slow clearing biomolecules such as peptide conjugates, antibodies, and nanoparticles [8]. This compatibility of the biological half-life of the bioconjugates with the radioactive half-life of the elements results in improved signal to background ratios. Conceptually, radio-labeling a protease substrate with two SPECT compatible radioisotopes that emit gamma rays at different energies could provide a new approach for molecular imaging of protease activities *via* ratiometric SPECT imaging. For this approach to be successful, gamma ray(s) of the chosen nuclides should have minimal overlapping signal in the acceptance energy windows to minimize "crosstalk." For practical reasons, this is not always achievable, leading to the use of radionuclides with significant crosstalk that must be removed in a quantifiable and reproducible manner. Another immediate challenge is to ensure the dual radio-labeling of a single substrate for ratio-SPECT imaging. In the proposed strategy, the selective hydrolysis of an amide bond by the targeted protease will result in the trapping of one radionuclide in cells, while the other radionuclide is effluxed.

Based on these considerations, we have developed a molecular framework for developing and using dual radionuclide-labeled SPECT imaging agents for the molecular imaging of aberrant intracellular or extracellular proteases. Determining therapeutic response can help identify nonresponders at early time points, giving an opportunity to apply an alternative and potentially more effective treatment [9]. In this study, we demonstrated the application of the method by targeting intracellular executioner caspases responsible for induction of apoptosis, and thus are useful for monitoring the early response of tumors to treatment [10, 11]. Two caspase-3 cleavable peptides were radiolabeled with different SPECT radionuclides and evaluated *in vitro* and *in vivo* with single or dual SPECT isotopes, ^{125}I with ^{99m}Tc or ^{111}In. Acquisition parameters for small animal NanoSPECT imaging were developed for real-time dual-isotope SPECT image analysis. Results demonstrate the potential of using multiradionuclide-resolving power of clinically useful SPECT for noninvasively monitoring treatment response.

Materials and Methods

The chelator DOTA-tris(t-Bu ester) was purchased from Macrocyclics (Dallas, TX, USA). Acetic anhydride, *N,N*-diisopropylethylamine, trifluoroacetic acid (TFA), acetonitrile (ACN), piperidine, anisole, and dimethylformamide (DMF) were purchased from Sigma Aldrich (St. Louis, MO, USA). All the Fmoc amino acids, hydroxybenzotriazole (HOBt), and 2-(1H-benzotriazole-1-yl)-1,1,3,3-tetramethyluronium hexafluorophosphate (HBTU) were purchased from AAPPtec (Louisville, KY, USA). Na [^{125}I]Iodide was ordered from American Radiolabeled Chemicals, Inc. (St. Louis, MO, USA), [^{111}In]$InCl_3$ was ordered from Nordion Inc. (Ottawa, ON, Canada), and ^{99m}Tc was obtained from Mallinckrodt Pharmaceuticals, St. Louis.

Synthesis of LS370 and LS734 and radiochemistry are described in the supplemental file.

Caspase-3 Mediated Hydrolysis of [^{125}I]LS370

[^{125}I]LS370 was dissolved in caspase buffer {100 mM NaCl, 50 mM 4-(2-hydroxyethyl)-1-piperazineethanesulfonic acid, 10 mM DTT, 1 mM ethylenediaminetetraacetic acid, 10 %

Author Manuscript Author Manuscript Author Manuscript Author Manuscript

glycerol, and 0.1 % 3-[(3-cholamidopropyl) dimethylammonio]-1-propanesulfonate, pH 7.4} at concentrations varying from 2.5 to 20 μM. Caspase-3 (Cal Biochem) was added to the radioactive peptide solution at a final concentration of 290 pM. These solutions were allowed to react at 37 °C for 180 min and were sampled every 30 min. Substrate hydrolysis was monitored by radio-high-performance liquid chromatography (Vydac, C-18, 4.6×250 mm, 1 ml/m, A=$H_2$0, 0.1 % TFA, B=ACN, 0.1%TFA; 10–90 % B, 30 min, linear gradient) of these time point samples. Comparison to a standard caspase-3 substrate (Ac-DEVD-pNA) and calculation of the enzyme kinetic parameters were carried out as previously described [12].

Cell Uptake and Efflux Studies With [^{125}I]LS734 or [^{125}I]LS370

Tissue culture protocol is described in the supplemental file. MDA-MB-231 cells used for the uptake and efflux assay were grown on 24-well tissue culture plates until they were 80–90 % confluent with ~250,000 cells per well. A two-component chemotherapeutic regimen was used that has been shown to initiate apoptosis in breast cancer cells and xenografts [13, 14]. The experimental treatment group of cells was treated with 10 ng/ml of SN-38 (7-ethyl-10-hydroxycamptothecin, Sigma Aldrich) for 24 h. Then, the SN-38 was removed, and the second chemotherapeutic drug, UCN-01 (Sigma Aldrich), was introduced at a concentration of 1 μM in 0.1 % BSA per well. At this point, respective radioactive solutions ([^{125}I]LS734 or [^{125}I]LS370, 0.02 μg per well; specific activities: [^{125}I]LS370—40×10^6 MBq/mmol; [^{125}I]LS734—10×10^6 MBq/mmol) were added to treated and control groups. The solutions were added drop-wise into the wells and gently mixed to ensure homogeneous distribution. The final volume per well was 240 μl, and the plates were incubated at 37 °C (5 % CO_2) for 2 h. After incubation, the supernatant (fraction 1) was collected, and the cells were washed twice with 250 μl of cold serum-free media. The washed cells were incubated again for 1 h in serum-free media at 37 °C (5 % CO_2), and at 1 h, the supernatant was collected (fraction 2). Fraction 2 represents the cell efflux, which is the amount of radioactivity released from cells after the 2 h uptake. After collecting the supernatant, Solvable (PerkinElmer) was added to facilitate efficient scraping of the cells. The scraped cells (fraction 3) were collected in microfuge tubes. The radioactivity in each fraction was measured in a well counter (Packard II gamma counter).

Animal Biodistribution Studies

All animal studies were conducted according to guidelines on the humane care and use of laboratory animals under protocols approved by the Animal Studies Committee at Washington University School of Medicine. For tissue biodistribution studies, syngeneic breast tumor models were prepared *via* bilateral orthotopic implantation of luciferase-transfected 4T1 mouse mammary carcinoma cells (4T1*luc*, 5×10^5 cells per tumor) in the mammary fat pads of 6-week-old, female Balb/c mice (NCI, Frederick, MD, USA). Studies were conducted when the tumors reached about 3 mm maximum diameter (~10 days). Healthy female Balb/c mice (n=4 per time point) were anesthetized with 1–2 % vaporized isoflurane and injected *via* tail vein with 0.185 MBq of [^{125}I]LS370 or [^{125}I]LS734 (specific activities: [^{125}I]LS370—40×10^6 MBq/mmol; [^{125}I]LS734—10×10^6 MBq/mmol). At 1 h postinjection, mice were killed. Organs of interest were removed and blotted dry. The radioactivity was measured in a gamma counter (Packard II gamma counter). Diluted

Author Manuscript Author Manuscript Author Manuscript Author Manuscript

standard doses (1:100) were prepared and counted along with the samples. Data points were corrected for radioactive decay. The percent injected dose per gram of tissue (%ID/g) was calculated.

Dual ^{125}I-^{111}In Nuclides SPECT Imaging Phantom and Animal Imaging

Phantom studies were designed based on the half-life decay of ^{125}I [$t_{1/2=59.4}$ days; X-ray: ~27.3 keV (145.2 %)] and ^{111}In [$t_{1/2}$=2.8 days; X-ray, ~23 keV (82.5 %) and γ-ray, 171 keV (90.6 %), 245 keV (94.1 %)]. The data were acquired in two energy windows, a low-energy window for ^{125}I (25.2–30.8 keV) and a second encompassing the two high energy peaks of ^{111}In (140–260 keV) using the NanoSPECT/CT system (Bioscan). As a consequence of this dual-labeling strategy, ^{125}I measurements were contaminated with ^{111}In activity due to overlap in the X-ray energy and contamination from down scatter (photons emitted by the higher energy isotope in the energy window of the lower energy isotope). Therefore, a strategy for unmixing of the overlapping gamma ray energy signals was formulated. An unmixing strategy based on the makeup of signals in each collection window (M_{I} and M_{In}) was developed:

$$\begin{aligned} M_{\mathrm{I}} &= e_{\mathrm{I}}[\mathrm{I}] + e_{\mathrm{InX}}[\mathrm{In}] + C_{\mathrm{In9I}}[\mathrm{In}] \text{ and } M_{\mathrm{In}} \\ &= e_{\mathrm{In}}[\mathrm{In}] + C_{\mathrm{I9In}} \end{aligned} \quad (1)$$

with e_{I} and e_{In} representing the detection efficiencies for ^{125}I and ^{111}In in their respective window and e_{InX} the efficiency for detecting the indium X-rays in the ^{125}In window. $C_{\mathrm{In>I}}$ and $C_{\mathrm{I>In}}$ are the cross-talk contamination factors from ^{111}In into the ^{125}I window and from 125I into the ^{111}In window. Under these conditions, e_{InX} cannot be separated from $C_{\mathrm{In>I}}$. $C_{\mathrm{I>In}}$ should be small. $C_{\mathrm{In>I}}$ is the sum from the down scatter from the 171 and 245 keV gamma rays and X-rays efficiency of ^{111}In in the ^{125}I window. Therefore:

$$\begin{aligned} [\mathrm{In}] &= (e_{\mathrm{I}} M_{\mathrm{In}} - C_{\mathrm{I9In}} M_{\mathrm{I}}) / (e_{\mathrm{I}} e_{\mathrm{In}} - C_{\mathrm{I9In}} C_{\mathrm{In9_I}}) \text{ and } [\mathrm{I}] \\ &= (M_{\mathrm{I}} - C_{\mathrm{In9I}} M_{\mathrm{In}}) / e_{\mathrm{I}} \end{aligned}$$

The phantoms were made of two ampoules containing a calibrated amount of ^{111}In (87 μCi) and ^{125}I (76 μCi). The three-dimensional (3D) regions-of-interest (ROIs) were drawn to encompass the entire ampoules. The dual-isotope SPECT/CT imaging in spontaneous breast cancer model is described in the supplemental text.

Data analysis and statistics are described in the supplemental file.

Results

Synthesis of Caspase-3 Containing Peptide Biomolecules for Imaging Apoptosis

The primary consideration of the molecular design is to ensure that each molecule can be labeled with two energetically different SPECT radionuclides. Thus, the basic structural framework consists of a peptide substrate for the target protease and reactive motifs to selectively incorporate the radionuclides at opposite ends of the peptides. Cleavage of the peptide substrate will alter the biodistribution profiles of the ensuing fragments. By determining the kinetics of each radiative fragment following cleavage, a ratiometric SPECT

Author Manuscript Author Manuscript Author Manuscript Author Manuscript

technique can be developed to report the activity of target enzymes. In this study, we designed molecular imaging probes that are sensitive to the activity of the executioner caspases (caspase-3/7). These caspases, which are upregulated in the early phase of caspase-mediated cell death, recognize and cleave the tetrapeptide motif, DEVD (aspartic acid–glutamic acid–valine–aspartic acid). To illustrate the concept, we designed two molecular imaging agents, LS370 and LS734 (Fig. 1), containing this motif. Both peptides were prepared by modular solid-phase synthesis. LS370, which contains only nine amino acid peptide sequence, is a simple model of the dual radiolabeled molecular imaging agent for ratiometric SPECT. It consists of DEVD peptide flanked by a tyrosine group for ^{125}I labeling and –Lys–Gly–Cys– group for ^{99m}Tc labeling. The more elaborate analogue, LS734, was designed to generate disparate molecular features upon enzyme cleavage to facilitate ratiometric SPECT data analysis. LS734 comprises 21 amino acids and consists of three functional components: (a) a cell internalizing (positively charged) amino acid sequence capable of accommodating stable ^{111}In [Gly–Arg–Arg–Arg–Orn–Arg–Arg–Lys–Lys–Arg–Lys–(−DOTA)–NH_2], (b) a caspase-3 cleavable DEVD peptide sequence, and (c) a hydrophobic peptide sequence containing Tyr group for labeling with ^{125}I (Ac–Tyr–Leu–Ala–Ile–Ahx–Pro–Ala). All the peptides were obtained in high purity (>95 %) by high-performance liquid chromatography and characterized by liquid chromatography–mass spectrometry. Upon cleavage, LS734 is expected to dissociate into ^{125}I-labeled hydrophobic and ^{111}In-labeled hydrophilic fragments, with distinct biodistribution profiles. Conceptually, the high disparity between the hydrophobic and the positively charged hydrophilic peptide fragments ensures a relatively higher efflux rate of one of the fragments from cells undergoing caspase-mediated apoptosis than the other component. Optimization of the biological transport profiles can be achieved by incorporating molecules that facilitate active efflux of one fragment.

Radiochemistry

The achieved specific activities were as follows: [^{125}I]LS370, 40–50×10^6 MBq/mmol; [^{125}I]LS734, 6–10×10^6 MBq/mmol; and [^{111}In]LS734, 12×10^6 MBq/mmol. The specific activity of [^{125}I]–[^{111}In]LS734 was 3×10^6 MBq/mmol. We also determined the specific activity of [^{99m}Tc]LS370 from the purified [^{125}I]–[^{99m}Tc]LS370. Based on a specific activity of 50×10^6 MBq/mmol of ^{125}I-LS370, the specific activity of ^{99m}Tc in [^{125}I]–[^{99m}Tc]LS370 was calculated. After 72 h of decay, 0.02 % of ^{99m}Tc remained, but this fraction did not have a significant impact on the ^{125}In counting window (15–75 keV). Based on the sum of the counts per minute (CPM) from fractions 10–12 and the counting efficiency (0.679 CPM/DPM; see Supplemental Fig. 1), the calculated specific activity of 99mTc in [^{125}I]–[^{99m}Tc]LS370 was 17×10^{10} MBq/mmol. This value is in good agreement with the literature reported maximum specific activity of 99mTc, which is ~20×10^{10} MBq/mmol [15].

Dual [^{125}I]–[^{111}In] Nuclide SPECT Imaging Phantom

The data were acquired in two energy windows, one at 30 keV of ^{125}I and a second encompassing the two high energy peaks of ^{111}In (171 and 245 keV). The consequence of this dual-labeling strategy is that ^{125}I measurements are contaminated with ^{111}In activity due to overlap in the X-ray energy and contamination from down scatter. Based on the unmixing

Author Manuscript Author Manuscript Author Manuscript Author Manuscript

strategy described in “Materials and Methods,” efficiency and cross-contamination factors were determined by scanning of the calibration phantoms containing known activities of ^{125}I and ^{111}In (Fig. 2; Tables 1 and 2). The 3D ROIs drawn on the entire ampoules and unmixed images were calculated by the arithmetic on the images, not from the ROI data.

Caspase-3 Mediated Hydrolysis

Figure 3 shows that [^{125}I]LS370 eluted at 19.5 min, and in the presence of caspase-3, the cleaved fragments eluted at 12.5 and 13 min. The presence of two radiolabeled peaks on the radiochromatogram suggests the formation of dimer caused by the expected oxidation of the thiol group to form intermolecular disulfide bond. However, the dimer readily converts back to single molecules under the high reducing conditions such as used to prepare the 99mTc chelate. Kinetic analysis of caspase-3 activation with [^{125}I]LS370 using a radionuclide detector (radio-high-performance liquid chromatography) gave a K_M and k_{cat} of 15±3 μM and 1.02±0.06 M s^{-1}, respectively. These parameters compared favorably with a standard caspase-3 substrate Ac-DEVD-pNA (K_M=11 μM and k_{cat} =2.4 M s^{-1}), demonstrating that the radiolabeled peptide was recognized by caspase-3.

Cell-Uptake Assays

The goals of the cell-uptake studies were to (1) assess any changes in the structure–activity relationship resulting from the modular and responsive probe design and (2) evaluate the retention of the iodine containing hydrophobic peptide moiety in treated and untreated cells. Metastatic human breast MDA-MB-231 cells were used to evaluate whether the amino acid sequence modulation would enhance internalization, and how the probe would respond (intracellular) postchemotherapy. In the untreated cells, there was a higher uptake (P<0.001) of [^{125}I]LS734 (3.6±0.5) than [^{125}I]LS370 (0.3±0.3) at 2 h postincubation at 37 °C (Fig. 4a). The same trend was observed with the treated cells. The amount of iodinated fraction released by the untreated and treated cells at 3 h (post 2 h incubation and removal of excess activity) was used as a measure of the efflux activity. The results showed that higher amount of activity was released from untreated cells compared to treated cells that had been incubated with [^{125}I]LS734 (P<0.001) (Fig. 4b).

Biodistribution

The structure–activity relationship was evaluated *in vivo* by performing a tissue biodistribution study in naive (Supplemental Fig. 2) and tumor-bearing Balb/c mice (Fig. 5). At 1 h, [^{125}I]LS734 circulated longer in blood as compared to [^{125}I]LS370. The tumor/blood ratios for both [^{125}I]LS370 and [^{125}I]LS734 was 0.6±0.03. The tumor/muscle ratios were similar as well but higher than the tumor/blood ratios, [^{125}I]LS734 (2.2±0.1) and [^{125}I]LS370 (2.1±0.3). Thyroid uptake was 73±21and 115±73 for [^{125}I]LS370 and [^{125}I]LS734, respectively.

Dual-SPECT Imaging of Spontaneous Breast Tumor Mouse Model After Injection of [^{125}I]–[^{111}In]LS734

Based on the results obtained for the unmixing of ^{125}I and ^{111}In detection windows in calibration phantoms, a proof-of-principle *in vivo* imaging study was performed using the

Author Manuscript Author Manuscript Author Manuscript Author Manuscript

dual radiolabeled [^{125}I]–[^{111}In]LS734 to determine the tumor response to therapy in a MMTV-PyMT transgenic mouse model of spontaneous breast cancer. Reconstruction of raw data from both the low- and high-energy collection windows demonstrated differential biodistribution of [^{125}I]–[^{111}In]LS734 throughout the animal (Fig. 6). At early time points, high uptake of an iodinated moiety, resulting from the deiodination of the parent compound, was observed in the thyroid glands. Rapid clearance of ^{111}In peptide conjugate was indicated by high activity in the kidneys and bladder. Sequential analysis by unmixing of the low-energy window further differentiated the biodistribution of ^{125}I- and ^{111}In-labeled compound and its fragments. Some tumor-independent proteolysis of the compound is expected due to minor activity of caspases and proteases in other tissues, particularly the liver and the kidneys. Early clearance of the ^{125}I-labeled moieties is evident by the relatively high signal from the gastrointestinal tract in the low-energy window (Fig. 6c). While the iodine containing component was designed to be hydrophobic upon cleavable and separation from the parent compound, the ^{111}In containing fraction was conceptualized to be hydrophilic following separation from the dual-labeled peptide. Although partial clearance from the liver was observed, the high signal from the kidneys and bladder demonstrated preferential renal to hepatobiliary clearance for the ^{111}In containing fragments. SUV analysis of the drug-treated and saline-treated tumors showed higher signal in the ^{111}In channel for the treated (SUV, 2.21) as compared to untreated (SUV, 1.44) tumor. The SUV analysis in the ^{125}I channel was also quantifiable but confounded by systemic deiodination (treated SUV, 0.19 and saline-treated SUV, 0.21). The *ex vivo* biodistribution corroborated the *in vivo* image analysis (Supplemental Fig. 3).

Discussion

In the preclinical arena, optical imaging has been used to report a plethora of molecular processes. With its diverse contrast mechanisms, optical imaging is amenable to high throughput screening, real-time feedback, and highly sensitive detection schemes without the use of ionizing radiation or expensive imaging systems. A unique feature of optical imaging is the detection of the expression and the functional status of proteases with high detection sensitivity using activatable reporter probes. Particularly, the commonly used Forster resonance energy transfer (FRET) method for imaging proteases is attractive for studying the functional status of these enzymes because of the near-zero background fluorescence before enzyme activation, resulting in high detection sensitivity and specificity [16–19]. Despite its enormous potential to unravel the molecular basis of diseases *in vivo*, the limited tissue penetration depth precludes using optical imaging techniques for noninvasive imaging of deep-seated primary and metastatic tumors.

Although radionuclide signal cannot be quenched or amplified in the same manner as fluorescence activatable probes, direct readout of protease activity can be achieved by ratiometric SPECT approach. To accomplish this goal, we have designed a dual radionuclide-labeled molecular probe and a SPECT imaging approach for quantitative measurement of protease activity. Our approach is versatile, with potential application in determining the functional status of both intracellular and extracellular proteases. Using a caspase-3 cleavable peptide sequence, we demonstrated that the chemical scaffold on the molecules can be used to alter the cellular internalization and efflux profile of the

Author Manuscript Author Manuscript Author Manuscript Author Manuscript

compounds. For example, the presence of positively charged amino acid residues in LS734 significantly enhanced cell internalization relative to LS370. Further, the ratio of retained activity from the hydrophobic moiety of ^{125}I-LS734 was higher in the treated cells *in vitro* versus nontreated cells.

Quantitative accuracy and statistical reconstruction for dual-SPECT isotopes was developed using the available NanoSPECT image reconstruction software. The software design offers select options for three parameters: background correction (in projection data) prior to reconstruction (low, medium, and high), number of iterations (fast, standard, and fine corresponding to 6, 9, and 21 ML-EM iterations), and the pixel size (0.2, 0.3, and 0.4 mm). The standard parameters are low background correction, 9 iterations, and 0.3 mm pixel size. The reconstruction software for the NanoSPECT was evaluated at various scan durations (i.e., counting statistics) with various options within the reconstruction such as the background clean (BC), smooth projection (SP), and smooth volume (SV) using a uniform phantom. We demonstrated that the different levels of background correction (low, medium, and high) did not make any difference in the image. Furthermore, the noise properties for these parameters were identical, as seen on the images using the standard number of iterations (9) and the standard pixel size (0.3 mm; see Supplemental Fig. 4). We postulated that the background subtraction was needed to be used in conjunction with the BC option to make a difference. We also observed that the BC option preserved the highest accuracy since the mean ROI values at various scan durations match closely to the reference mean ROI value (i.e., value obtained from the highest counting statistics) compared to the reconstruction with the other options. However, at the lowest counting statistics, the BC option produces the lowest accuracy. This is probably due to bias generated from the background subtraction at low counts. In contrast, the default reconstruction with no additional option produces the highest accuracy at the lowest counting statistics compared to the rest. With regard to the coefficient of variation (STD/mean) of the ROI values (Supplemental Fig. 5), the BC option showed the highest variation as expected, whereas the SP option depicts the lowest.

The pharmacokinetic profile in rodents demonstrated the differences in the blood circulation and tissue retention of the bioconjugates. Proof-of-principle animal imaging was performed in the MMTV-PyMT transgenic breast cancer model using the phantom validated customized attenuation and gamma-energy deconvolution SPECT/CT protocols. Cell studies demonstrated differences in the uptake of the dual radiotracer between the treated and nontreated groups. The iodine label was stable in the conditions used for the cell studies (Supplemental Fig. 6). However, a key limitation of compound design was the significant ^{125}I uptake in the thyroid tissue, most likely a function of normal as well as tumor mediated physiologic deiodination caused by the labile carbon–iodine bond [20]. In designing the dual radiolabeled imaging agent, we expected that the intracellular caspase-3 cleavage of the multifunctional molecular agent would result in the trapping of the ^{125}I-labeled hydrophobic component, while the ^{111}In-labeled moiety will be cleared. Clearly, deiodination confounded accurate systemic data analysis. In the ^{111}In channel, the SUV analysis of the drug- and saline-treated tumors showed higher signal for treated (2.21) *versus* untreated tumors (1.44). In spite of *in vivo* deiodination, quantitative ROI analysis of various tissues in the ^{125}I channel was feasible using the described algorithm. The proof-of-principle

Author Manuscript Author Manuscript Author Manuscript Author Manuscript

animal study and the phantom studies have laid the foundation for future noninvasive dual radionuclide SPECT studies for imaging intracellular protease activity in response to treatment using biostable imaging probes. We are currently designing imaging agents that better shield the radio-halogen from systemic enzymatic cleavage [21].

Conclusion

We developed a new approach for imaging protease activity *in vivo* via a ratiometric SPECT imaging strategy. The synthetic method is modular, which facilitates adaptation of the method to monitor the activities of other diagnostic proteases. Attenuation correction parameters for image reconstruction and quantitative analyses were optimized using phantoms, and successfully implemented for multispectral SPECT image analysis. By modeling the crosstalk between radioisotopes, the SPECT method provides quantitative accuracy for determining the ratios of each radionuclide. This strategy can potentially be adapted to current clinical imaging systems to provide a direct measure of diagnostic molecular biomarkers of early response to therapy.

Supplementary Material

Refer to Web version on PubMed Central for supplementary material.

Acknowledgments

We thank Rui Tang, Kvar Black, and Mingzhou Zhou for helpful discussions.

Funding. This work was funded primarily by grant from the Department of Defense Breast Cancer Research Program (W81XWH-09-1-0333) and supported in part by grant from the National Institutes of Health NIBIB R01 EB021048 and resources from the Washington University Molecular Imaging Center (NCI P50 CA094056). WJA is supported in part by an award from the NIH Office of Research Infrastructure Programs (K01RR026095). MS is supported in part by an R01 award from NIH (R01CA176221).

References

1. Choi KY, Swierczewska M, Lee S, Chen X. Protease-activated drug development. Theranostics. 2012; 2:156–178. [PubMed: 22400063]
2. Boya P, Kroemer G. Lysosomal membrane permeabilization in cell death. Oncogene. 2008; 27:6434–6451. [PubMed: 18955971]
3. Johansson AC, Appelqvist H, Nilsson C, et al. Regulation of apoptosis-associated lysosomal membrane permeabilization. Apoptosis. 2010; 15:527–540. [PubMed: 20077016]
4. Graham MM. Clinical molecular imaging with radiotracers: current status. Med Princ Pract: Int J Kuwait University, Health Sci Centre. 2012; 21:197–208.
5. Benard F, Turcotte E. Imaging in breast cancer: single-photon computed tomography and positron-emission tomography. Breast Cancer Res. 2005; 7:153–162. [PubMed: 15987467]
6. Chen DL, Zhou D, Chu W, et al. Radiolabeled isatin binding to caspase-3 activation induced by anti-Fas antibody. Nucl Med Biol. 2012; 39:137–144. [PubMed: 22033021]
7. Beekman F, van der Have F. The pinhole: gateway to ultra-high-resolution three-dimensional radionuclide imaging. Eur J Nucl Med Mol Imaging. 2007; 34:151–161. [PubMed: 17143647]
8. Edwards WB, Akers WJ, Ye Y, et al. Multimodal imaging of integrin receptor-positive tumors by bioluminescence, fluorescence, gamma scintigraphy, and single-photon emission computed tomography using a cyclic RGD peptide labeled with a near-infrared fluorescent dye and a radionuclide. Mol Imaging. 2009; 8:101–110. [PubMed: 19397855]

Author Manuscript Author Manuscript Author Manuscript Author Manuscript

9. Yang TJ, Haimovitz-Friedman A, Verheij M. Anticancer therapy and apoptosis imaging. Exp Oncol. 2012; 34:269–276. [PubMed: 23070012]
10. Wang J, Lenardo MJ. Roles of caspases in apoptosis, development, and cytokine maturation revealed by homozygous gene deficiencies. J Cell Sci. 2000; 113(Pt 5):753–757. [PubMed: 10671365]
11. Ashkenazi A, Dixit VM. Death receptors: signaling and modulation. Science. 1998; 281:1305–1308. [PubMed: 9721089]
12. Zhang Z, Fan J, Cheney PP, et al. Activatable molecular systems using homologous near-infrared fluorescent probes for monitoring enzyme activities *in vitro*, *in cellulo*, and *in vivo*. Mol Pharmaceutics. 2009; 6:416–427.
13. Ma CX, Cai S, Li S, et al. Targeting Chk1 in p53-deficient triple-negative breast cancer is therapeutically beneficial in human-in-mouse tumor models. J Clin Investig. 2012; 122:1541–1552. [PubMed: 22446188]
14. Bullok KE, Maxwell D, Kesarwala AH, et al. Biochemical and *in vivo* characterization of a small, membrane-permeant, caspase-activatable far-red fluorescent peptide for imaging apoptosis. Biochemistry. 2007; 46:4055–4065. [PubMed: 17348687]
15. Eckelman WC, Bonardi M, Volkert WA. True radiotracers: are we approaching theoretical specific activity with Tc-99m and I-123? Nucl Med Biol. 2008; 35:523–527. [PubMed: 18589295]
16. Chau I, Rigg A, Cunningham D. Matrix metalloproteinase inhibitors—an emphasis on gastrointestinal malignancies. Crit Rev Oncol Hematol. 2003; 45:151–176. [PubMed: 12604127]
17. Luker GD, Luker KE. Optical imaging: current applications and future directions. J Nucl Med. 2008; 49:1–4. [PubMed: 18077528]
18. Ntziachristos V, Bremer C, Graves EE, Ripoll J, Weissleder R. *In vivo* tomographic imaging of near-infrared fluorescent probes. Mol Imaging. 2002; 1:82–88. [PubMed: 12920848]
19. Bremer C, Tung CH, Weissleder R. *In vivo* molecular target assessment of matrix metalloproteinase inhibition. Nat Med. 2001; 7:743–748. [PubMed: 11385514]
20. Glazer DI, Brown RK, Wong KK, Savas H, Gross MD, Avram AM. SPECT/CT evaluation of unusual physiologic radioiodine biodistributions: pearls and pitfalls in image interpretation. Radiographics. 2013; 33:397–418. [PubMed: 23479704]
21. van Schaijk FG, Broekema M, Oosterwijk E, et al. Residualizing iodine markedly improved tumor targeting using bispecific antibody-based pretargeting. J Nucl Med. 2005; 46:1016–1022. [PubMed: 15937314]

Author Manuscript Author Manuscript Author Manuscript Author Manuscript

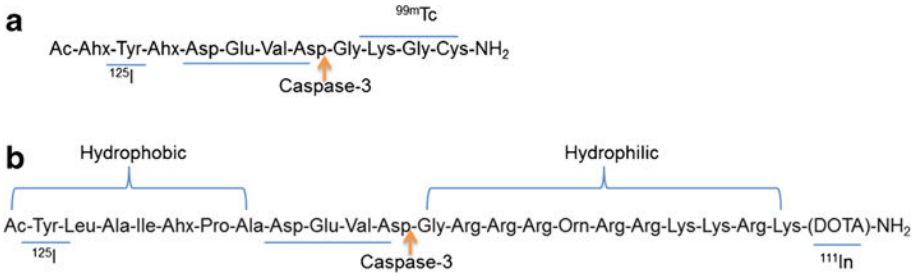

Fig. 1.
Structures of LS370 (**a**) and LS734 (**b**).

Author Manuscript Author Manuscript Author Manuscript Author Manuscript

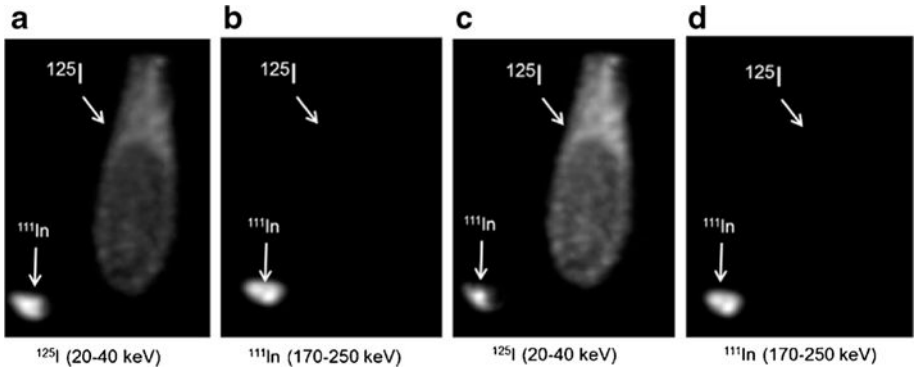

Fig. 2.

Vials containing either ^{125}I or ^{111}In were scanned with SPECT/CT. Raw (**a**, **b**) and unmixed (**c**, **d**) images were constructed from signals collected in two energy windows (20–40 keV and 170–250 keV).

Author Manuscript Author Manuscript Author Manuscript Author Manuscript

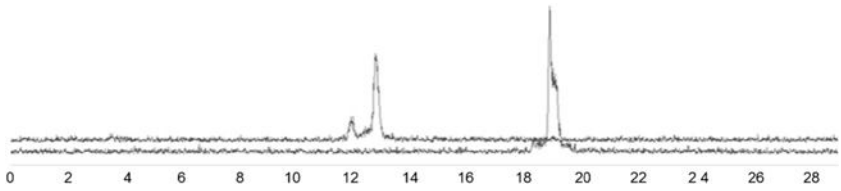

Fig. 3.

Radiochromatogram of [^{125}I]LS370 hydrolysis by caspase-3 (90 min). The [^{125}I]LS370 eluted at 19.5 min. Cleaved fragments eluted at 12.5 and 13 min.

Author Manuscript Author Manuscript Author Manuscript Author Manuscript

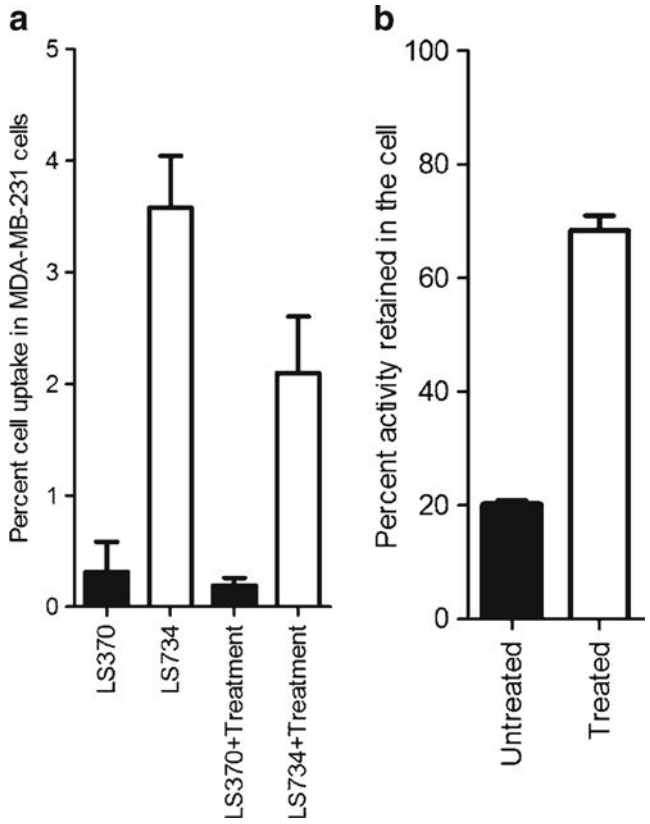

Fig. 4.

a Cell-uptake of [^{125}I]LS370 and [^{125}I]LS734 after 2 h incubation in the presence and absence of treatment. **b** Efflux profile of [^{125}I]LS734.

Author Manuscript Author Manuscript Author Manuscript Author Manuscript

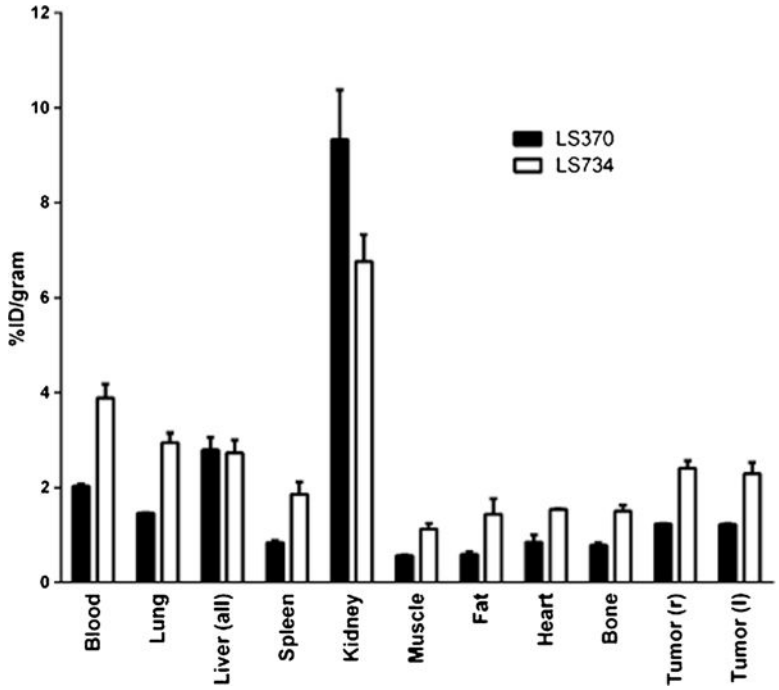

Fig. 5.

Tissue bio-distribution of [^{125}I]LS370 and [^{125}I]LS734 1 h after administration of 4–7 μCi of the respective radiopharmaceutical.

Author Manuscript Author Manuscript Author Manuscript Author Manuscript

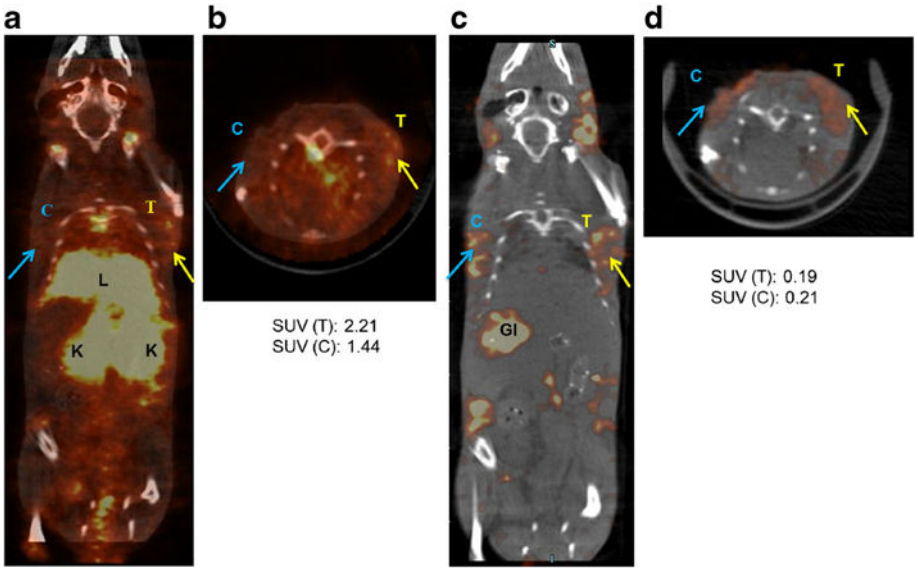

Fig. 6.

SPECT-CT images (single slice) after unmixing for high energy window for ^{111}In detection (170–250 keV) and for low energy window consisting of primarily ^{125}I activity (20–40 keV), collected at 4 h after injection of [^{111}In]–[^{125}I]LS734. **a**, **b** ^{111}In window: higher activity was detected in the treated tumor (*T*) than the saline control treated tumor (*C*). The kidneys (*K*) had highest signal followed by the liver (*L*) indicating fast clearance of the ^{111}In labeled probe and fragments. **c**, **d** ^{125}I window: activity was detected in both tumors, presumably preferential retention of the lipophilic fragment although activity gastrointestinal tract (*GI*) and thyroid glands indicates partial physiological deiodination, most likely a function of normal as well as tumor mediated. Therefore, reported SUV values for ^{125}I include peptide-bound and free fractions. High activity in the liver and GI indicates hepatobiliary clearance of the lipophilic ^{125}I fragments.

Author Manuscript

Author Manuscript

Author Manuscript

Author Manuscript

Table 1

Total activity counts from calibration images (Fig. 2) after unmixing ^{125}I and ^{111}In signals

Image	^{125}I ampoule	^{111}In ampoule
^{125}I	21.3	2.25
^{111}I	0.10	56.5

Author Manuscript

Author Manuscript

Author Manuscript

Author Manuscript

Table 2

Efficiency and cross-contamination factors

Factor	Measured/nominal	Value
e_{I}	21.29/76	0.280
e_{In}	56.47/87	0.650
$C_{In>I}$	2.25/87	0.026
$C_{I>In}$	0.10/76	0.001

The efficiency values represent the calibrated activities measured in the iodine or indium windows divided by the known activity of the sample